PERGAMON

Micron 30 (1999) 357–369

micron

www.elsevier.com/locate/micron

Towards quantitative measurements of charge transfer in complex crystals using imaging and diffraction of fast electrons

L. Wu, Y. Zhu*, J. Tafto[1]

Department of Applied Science, Brookhaven National Laboratory, Upton, NY 11973, USA

Received 22 October 1998; accepted 28 January 1999

Abstract

Electron diffraction and imaging are very sensitive to the valence-electron distribution in materials at small scattering angles. We take advantage of the large dimension of the unit-cell along the *c*-axis of $YBa_2Cu_3O_7$ and $Bi_2Sr_2CaCu_2O_{8+\delta}$ superconductors, to study the distribution of charge carriers, crucial to understanding the superconducting behaviors in these complex systems. Electron pile-up associated with a structural modulation in $Bi_2Sr_2CaCu_2O_{8+\delta}$ was imaged at an atomic resolution. Charge transfer normal to the *a*–*b* plane in $YBa_2Cu_3O_7$ and $Bi_2Sr_2CaCu_2O_{8+\delta}$ was accurately measured and plotted using formal valences as a reference. The results were compared with the electronic structures based on first principle calculations. © 1999 Published by Elsevier Science Ltd. All rights reserved.

Keywords: Quantitative electron diffraction and imaging; Charge density and charge transfer; Novel convergent beam electron diffraction; High-temperature superconductors

1. Introduction

Most bulk and microstructural properties of a material depend directly on the bonding between its constituent atoms. Thus, to provide a fundamental description of the physical behavior of a material, such as superconductivity, it is essential to understand its electronic structure on a subatomic scale, especially the spatial distribution of the valence electrons that bind the atoms together. The important correlation between the occurrence of superconductivity and the number of valence electrons, counting the number of electrons outside a filled inner-shell per atom, was first noticed by Matthias (1957). In high-temperature superconductors, electron holes are charge carriers. The holes are known to be confined to the CuO_2 plane, but their relationship to the magnetic and superconducting properties still remains elusive. The recent discovery of the charge stripes in high T_c superconductors and related materials (Tranquada et al., 1995) suggests that, below a certain temperature, the electronic carriers become localized onto specific sites, which display long-range order throughout the crystal structure to form charge ordering that is directly associated with the superconductivity mechanism. This observation once again pointed out the significance of understanding bonding, ionicity and valence-electron distribution in a crystal lattice. Nevertheless, our knowledge of crystal bonding and charge distribution is often derived from theory or indirect evidence rather than from direct experimental measurements. Meaningful experimental data can be obtained only when the accuracy in the measurement of the charge distribution is far higher than the difference between crystal models consisting of neutral atoms and ions. Accurate measurement of the distribution of the valence electrons are prerequisite to understand the superconducting properties of the cuprates from microscopic first principles.

The charge distribution between adjacent atoms, which depends on bond length and the symmetry of the atoms' arrangement and their electronic characteristics, determines the bonding and ionicity of the crystal. In general, the electronic structure and crystal structure are strongly coupled and they are constrained by each other. Electron distribution in materials are traditionally studied with X-ray diffraction techniques, and electronic energy levels and their symmetry by emission and absorption spectroscopy with incident X-rays and electrons (Nücker et al., 1989, 1995; Fink et al., 1994). In transmission electron microscopy (TEM), the limited studies of electronic structure in high-temperature superconductors have focused on the near-edge structure of the oxygen K-edge and the copper L-edge using electron

* Corresponding author. Tel.: + 1-516-344-3057; fax: + 1-516-344-4071.

E-mail address: zhu@bnl.gov (Y. Zhu)

[1] Visiting scientist from the Department of Physics, University of Oslo, Norway.

0968-4328/99/$ - see front matter © 1999 Published by Elsevier Science Ltd. All rights reserved.
PII: S0968-4328(99)00039-6

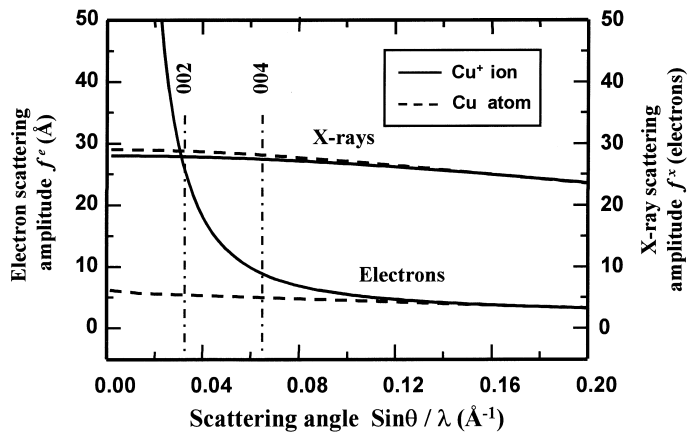

Fig. 1. Scattering amplitude of electron and X-ray diffraction, f^e and f^x, respectively, for the Cu atom and Cu^+ ion. The vertical dashed lines show the innermost reflection positions of Bi/2212. Note, the huge difference in sensitivity to the rearrangement of the valence electron at small scattering angles between electrons and X-rays.

energy-loss spectroscopy, mainly to utilize its small probe to study structural defects. The strength and uniqueness of the electron diffraction and imaging techniques in determining charge distribution in these complex crystals have not received the same attention. In this article, we first discuss the sensitivity of incident-electrons for detecting valence electrons in materials, and the great advantage and potential of studying charge distribution with TEM. As an example, we examine how the charge ordering in $Bi_2Sr_2CaCu_2O_{8+\delta}$ (Bi/2212) can be revealed in high-resolution images. We then describe a novel electron diffraction technique we developed recently (Zhu and Tafto, 1997; Tafto et al., 1998) to determine charge distribution by accurately measuring electron diffraction intensities as a function of crystal thickness, and the associated error analysis. Finally, we present the results of our measurements of the distribution of charge density and charge transfer in $YBa_2Cu_3O_{7-\delta}$ and Bi/2212 superconductors.

2. Charge density and charge transfer

A good approximation in the study of the electronic structure of materials is to assume that when atoms are put together to form a crystal, only the valence electrons are rearranged. The term "valence", which is sometimes ambiguous, in this sense describes the number of bonding electrons per atom; material chemists prefer the term "formal valence". For ionic crystals, the formal-valence assignment can be found in chemical tables, and that works well for the synthesis of oxides, for example, to explain many chemical and physical properties and phenomena. Frequently, electron-structure calculations agree with these assignments. Although high T_c oxides exhibit many metallic properties, the formal valence has been used to describe the actual ionic charge of the materials.

The spatial distribution of valence electrons can be measured experimentally. In X-ray and electron diffraction, the electron density of the diffracting crystal varies periodically along any direction through the lattice, similar to the periodic distribution of atoms. The electron density, ρ, at the point $\mathbf{r}$ in the unit-cell can be expressed as a Fourier series:

$$\rho(r) = \frac{1}{V}\sum_{\mathbf{g}} F^x_{\mathbf{g}} \exp(-2\pi i\mathbf{g}\cdot\mathbf{r}). \tag{1}$$

Here, V is the volume of the crystal unit-cell and $\mathbf{g}$ the reciprocal vector of the lattice planes. $F^x_{\mathbf{g}}$ is a Fourier coefficient, or the structure factor of the reflection g measured with X-rays, and is defined by:

$$F^x_{\mathbf{g}} = \sum_i f^x_i(s)\exp(-B_i s^2)\exp(-2\pi i\mathbf{g}\cdot\mathbf{r}) \tag{2}$$

where $s = \sin\theta/\lambda$, θ is the scattering angle and λ the wave length of the incident beam. f^x_i is the scattering amplitude of X-rays and B_i the Debye–Waller factor of the ith atom. If we use formal valence as a reference, the valence-electron distribution, or the charge transfer, can be determined directly by Fourier transform:

$$\Delta\rho(\mathbf{r}) = \rho_{\mathrm{m}}(\mathbf{r}) - \rho_{\mathrm{f}}(\mathbf{r}) = \frac{1}{V}\sum_{\mathbf{g}} (F^x_{\mathbf{g}\mathrm{m}} - F^x_{\mathbf{g}\mathrm{f}})\exp(-2\pi i\mathbf{g}\cdot\mathbf{r}). \tag{3}$$

Here, the subscript m refers to the ideally measured values of the X-ray structure factors, $F^x_{\mathbf{g}\mathrm{m}}$, and of the electron density $\rho_m(r)$ in the crystal, and f refers to the corresponding calculated values assuming atoms with assigned formal valence. In principle, if we can accurately measure $F^x_{\mathbf{g}\mathrm{m}}$, we should be able to determine the charge distribution. Charge distribution has been determined using X-ray and electron diffraction, but earlier only for systems with simple crystal structure and a small unit-cell, such as MgO (Zuo et al., 1997). The question we encountered was: does electron-, or X-ray-diffraction have sufficient sensitivity and accuracy to determine the structure factors that are sensitive to a

minute change of charge distribution in complex crystal with a large unit-cell?

3. The sensitivity of electron probe to valence electrons in crystals

3.1. Electron scattering amplitudes of a charged atom at small scattering angles

When an incident electron beam interacts with a crystal in a diffraction experiment, unlike X-rays that only see electrons surrounding an atom, the high-energy electrons with an energy range 100–1000 kV see the electrostatic potential of an atom with a positively charged nucleus screened by a negatively charged electron cloud. Thus, the scattering amplitude of an atom for incident electrons at small scattering angles is determined mainly by the net charge of the atom, rather than by the total density of electrons. In other words, the electrostatic potential is strongly influenced by ionicity and charge transfer in the crystal. The difference in sensitivity to charge transfer between electrons and X-rays can be revealed by the Mott formula:

$$f^{e}(s) = \frac{8\pi^2 m_0 e^2}{\hbar^2}\left(\frac{1}{s^2}\right)(Z - f^{x}) \tag{4}$$

where the superscript e denotes the scattering amplitude for electrons, corresponding to x for X-ray. Z is the charge of the nucleus, m_0 the rest-mass of an electron, $\hbar$ is Planck's constant, and e the charge on the electron. Since incident X-rays interact with electron clouds in materials, f^x is determined by the spatial distribution of electrons around the atom. Near the forward direction where f^x is close to Z, small changes in f^x can drastically alter f^e. For an individual charged atom, or an ion, the electron scattering amplitude near forward direction ($s \approx 0$) approaches infinity (see Fig. 1), but not for a crystal if the neutrality over a crystal unit-cell is considered (see Section 3.2). Fig. 1 compares the scattering amplitude of an electron and an X-ray diffraction for a Cu atom and a Cu^+ ion. For scattering angles smaller than say $s = 0.08$ Å^{-1}, there is a huge difference in sensitivity to the ionicity of an atom, i.e. the rearrangement of the valence electrons, between incident electrons and X-rays.

In high-temperature superconductors, the density of charge carriers, or electron holes is typically considerably less than 1% of the total density of electrons (294 electrons per unit-cell for $YBa_2Cu_3O_{7-\delta}$ and 1536 electrons for a Bi/2212 sub-unit-cell). This poses great difficulties in accurately determining the distribution of charge carriers using X-rays. On the other hand, $YBa_2Cu_3O_{7-\delta}$ and Bi/2212 have large crystal unit-cells, and their low-order reflections are at very small scattering angles. The 001 and 002 reflections of $YBa_2Cu_3O_{7-\delta}$, and the 002 and 004 reflections of Bi/2212, marked by the dashed lines in Fig. 1, are especially sensitive to the ionicity of electrostatic potential of the crystals. With the large unit-cells and high local concentration of electron holes in these superconductors, electron diffraction and imaging using these inner reflections are expected to reveal information on the charge distribution in these materials. By studying the intensity (amplitude and phase) of these reflections, or rather their structure factors, which can be determined by replacing the scattering amplitude of X-ray f_i^x with that of electron f_i^e in Eq. (2), we can map the valence-electron distribution in these superconductors.

3.2. Structure factors of ionic crystals near the forward direction ($s \approx 0$)

One controversy in electron diffraction concerns the scattering amplitude at small scattering angles. It appears difficult to accept that there is no singularity at $s = 0$ for an ionic crystal with overall charge neutrality because of the singularity for individual ions. Many electron microscopists have experienced the catastrophe that happens when the electrons are not conducted away so that the specimen gets charged up. We now show that this does not happen, if we consider a crystal unit-cell with charge neutrality. The atomic scattering amplitude near the forward direction can be expressed as:

$$f^{e}(s)_{s\to 0} = \frac{8\pi^2 m_0 e^2}{\hbar^2}\left(\frac{1}{s^2}\right)(Z - (Z + n - \kappa s^2)). \tag{5}$$

Here n is the number of valence electrons on the charged atom (positive for anions and negative for cations), and κ is a constant. Thus, the structure factor of the crystal in the forward direction is:

$$F_{000}^{e} = \frac{8\pi^2 m_0 e^2}{\hbar^2}\left(\frac{1}{s^2}\right)\sum_i -n_i + \kappa_i s^2. \tag{6}$$

Because of charge neutrality in the unit-cell, the sum over $n_i$is zero, and the structure factor becomes

$$F_{000}^{e} = \frac{8\pi^2 m_0 e^2}{\hbar^2}\sum_i \kappa_i,$$

which is a finite number. To demonstrate the validity of our argument, let us examine a simple ionic crystal, MgO. Based on the scattering amplitudes of Rez et al. (1994), we calculated its mean inner potential in the forward direction: $U_{000}^{MgO} = F_{000}/\pi V_c = 12.2$ V. To evaluate κ, we simply considered the difference in the X-ray scattering amplitudes of O^{2-} at $s = 0.05$ compared with $s = 0$, giving $\kappa = 164.64$. The same procedure was also used for the Mg^{2+} cation. The calculated mean inner is close to that measured using interferometry (Gajdardziska-Josifovska et al., 1993).

We note that although the scattering amplitude of the individual charged atoms approaches infinity for $s \approx 0$, the structure factor and the mean inner potential are finite, when the number of negative and positive elementary charges is equal. Nevertheless, in published tables on scattering amplitudes for incident electrons, one frequently encounters finite scattering amplitudes at $s = 0$ for ions;

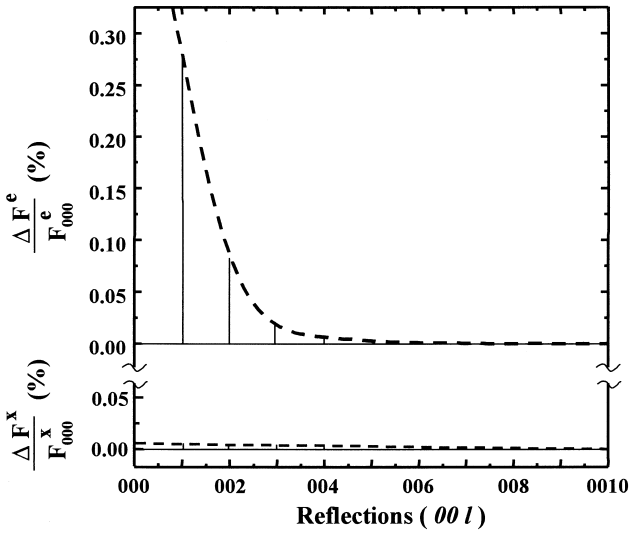

Fig. 2. 000-beam normalized difference-structure-factor $\Delta F/F_{000}$ (before and after moving 0.02 electron holes from the BaO plane to the CuO plane per $YBa_2Cu_3O_7$ unit-cell) as a function of the order of the 00*l* reflections for $YBa_2Cu_3O_7$. The vertical lines represent the position of the Bragg peaks (δ-function). Note, the scales of the vertical axis are the same for electrons and X-rays, showing that the electron diffraction has a greater sensitivity than X-ray diffraction to the valence-electron distribution in a crystal with Bragg reflections at a small reciprocal distance.

this is misleading because these tabulated values are not the real ionic-scattering amplitude of electrons at $s = 0$, but only the last term $(8\pi^2 m_0 e^2)/(\hbar^2)\cdot\kappa$ in Eqs. (5) and (6). We note that the problem of singularity for individual ions can be taken care of, when the Mott formula is used stringently by considering the whole crystal and by conversion from X-ray scattering amplitudes.

3.3. The effects of charge distribution and lattice displacement on structure factors

We measure amplitude and phase of reflections in electron diffraction experiments. For thin crystals, the intensity is proportional to $|F_{\mathbf{g}}|^2$. As shown in Eq. (2), the structure factor F_g can also be calculated if the scattering amplitude of the charged atom and atomic coordinates are known. Fig. 2 shows the change in calculated (00*l*) structure factor for electrons and X-rays, after moving 0.02 holes from the BaO plane to the CuO plane per $YBa_2Cu_3O_7$ unit-cell. The lines show the positions of Bragg reflections. Here, we define $\Delta F^e = F^e_c - F^e_n$ and $\Delta F^x = F^x_c - F^x_n$, and the additional subscript n and c refer to before and after the charge rearrangement, respectively. The F_{000} normalized difference in structure factors is huge for electron at small scattering angles, and it exponentially decay with the increase in the order of the reflections. (Note, moving 0.02 holes from CuO_2 to CuO plane gives the same trend; however, the 003 reflection intensity will be smaller than that of the 004, because the rearrangement of holes spans 1/3 of the unit-cell along the *c*-axis). In contrast, the difference in structure factor for X-ray is very small even for low-order reflections. It is clear that electron diffraction has a greater sensitivity than X-ray diffraction in addressing the valence-electron distribution in a crystal with the Bragg reflection at a small reciprocal distance.

Another advantage of studying charge distribution at small scattering angles in electron diffraction experiments is that the accuracy of the atomic coordinates becomes unimportant, i.e. a small lattice displacement only influences the intensity of reflections far out in the reciprocal space. This fact can be easily revealed by calculating the structure factor for a crystal with one atom being moved from r to $r + \Delta r$. For a centro-symmetric crystal with and without a small displacement Δr, the difference in structure factor $\Delta F_{\mathbf{g}}$ can be expressed as:

$$\begin{aligned}\Delta F_{\mathbf{g}} &= f_{\mathbf{g}} \exp 2\pi i\mathbf{g}\cdot(\mathbf{r} + \Delta\mathbf{r}) - f_{\mathbf{g}} \exp 2\pi i\mathbf{g}\cdot\mathbf{r}\\ &= f_{\mathbf{g}}(\cos 2\pi\mathbf{g}\cdot(\mathbf{r} + \Delta\mathbf{r}) - \cos 2\pi\mathbf{g}\cdot\mathbf{r}) - i f_{\mathbf{g}}(\sin 2\pi\mathbf{g}\cdot(\mathbf{r} + \Delta\mathbf{r})\\ &\quad - \sin 2\pi\mathbf{g}\cdot\mathbf{r})\\ &= -2f_{\mathbf{g}} \sin(\pi\mathbf{g}\cdot\Delta\mathbf{r})(\sin \pi\mathbf{g}\cdot(2\mathbf{r} + \Delta\mathbf{r}) + i \cos(\pi\mathbf{g}\cdot(2\mathbf{r} + \Delta\mathbf{r}))\end{aligned} \tag{7}$$

$$\left|\frac{\Delta F_{\mathbf{g}}}{f_{\mathbf{g}}}\right|^2 = \frac{\Delta F_{\mathbf{g}}\cdot\Delta F^*_{\mathbf{g}}}{f^2_{\mathbf{g}}} = 4\sin^2 \pi\mathbf{g}\cdot\Delta\mathbf{r}.$$

When the displacement Δr is small ($\mathbf{g}\cdot\Delta r \ll 1$), $\Delta F\mathbf{g}$ increases monotonically. To clearly demonstrate the trend of the variation in diffraction intensity with the reciprocal lattice $\mathbf{g}$, $\Delta F\mathbf{g}$ was normalized by the scattering amplitude $f\mathbf{g}$, and plotted in Fig. 3 with a displacement $\Delta r = 0.1\%$ of a unit-cell dimension along the *c*-axis. In the case of $YBa_2Cu_3O_7$, this displacement amounts to 0.011 Å. Fig. 3 shows the negligible change in the difference structure factor, or the difference intensity, due to the lattice displacement at small scattering angles ($s < 0.1$ Å^{-1}). Comparing

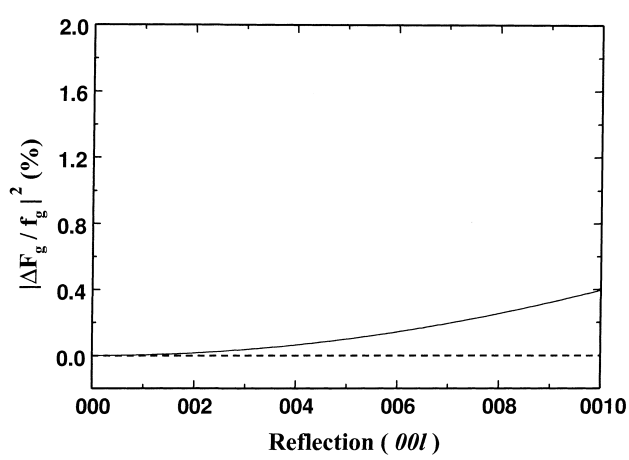

Fig. 3. Normalized difference in intensity $(\Delta F_g/f_g)^2$ (with and without a 0.1% lattice displacement along the *c*-axis) as a function of scattering angle, showing the effect of small displacement on structure factor.

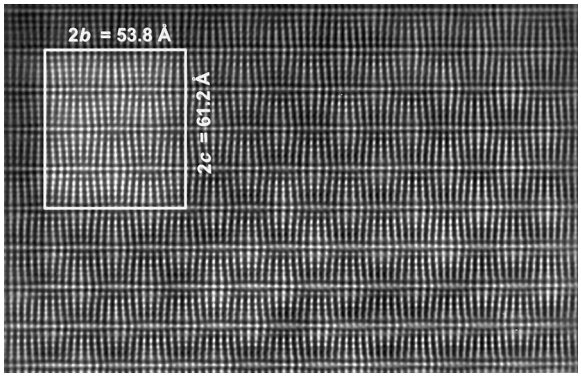

Fig. 4. An experimental HREM image of the displacive and charge modulation in Bi/2212, viewed along the [100]-axis. The embedded image (four superlattice cell) is the calculated one based on the structure model shown in Fig. 5(a). Crystal thickness of 2.7 nm and defocus of − 50 nm were used in the calculations. Note, the black-cage contrast represent pile-up of electrons.

Figs. 1 and 2 with Fig. 3, we note the complementarity of the displacement of atoms over short distances and the charge transfer over large distances. The significant influence of charge transfer on electron diffraction intensity occurs at small scattering angles, and displacement of atoms occurs at large scattering angles. X-ray and neutron diffraction intensities are similarly influenced by displacement of atoms, while the sensitivity at small angles to charge transfer is unique for electron diffraction.

4. High-resolution imaging of charge ordering

The key to imaging charge ordering using TEM is to use the high sensitivity of electron probe to the valence electron at small scattering angles. This is especially appealing for Bi/2212 superconductor which has a superlattice of dimensions $0.54 \times 2.6 \times 3.1\ nm^3$ due to its structural modulation. The low-order reflections associated with the superlattice, such as 011 and 002, are at very small scattering angles. Although HREM have played an important role in determining the atomic positions of the modulated structure since the discovery of Bi/2212 (Horiuchi et al., 1988), the periodic black-cage-like contrast associated with the double BiO layers observed in the *a*-axis projected atomic images (Fig. 4) has long puzzled researchers. The displacive nature of the modulation, apparently due to the insertion of extra oxygen O_δ in the BiO layer, is well established. Nevertheless, the modulation induced displacement, or the deviation in atomic coordinates from the sublattice of the crystal, as determined by neutron and X-ray diffraction (Imai et al., 1988; Gao et al., 1993), did not generate such contrast in calculated high-resolution images. Traditionally, experimental electron-diffraction patterns and electron-microscope images are compared with calculations, which assume that the atoms are neutral; in most cases this is a good approximation for small crystal unit-cells with interplanar spacings less than 0.5 nm, as demonstrated by Gemming et al. (1997). However, for a crystal with a large unit-cell, such as Bi/2212, this may not be so, and the effect of charge transfer over a long distance can be significant. The insertion of the extra oxygen O_δ in the BiO double layer certainly causes lattice displacement and rearrangement of the local charge distribution. To understand the charge component of the modulation, we focused on studying very thin areas of the crystal to minimize the multiple scattering experimentally, and also carried out dynamical calculations of electron diffraction and images using a multislice approach, and taking multiple scattering into account.

The model we used for the calculations was based on the charge assignment for Bi/2212 sublattice by Gupta and Gupta (1994) (see Table 1), however, we extended it into a three dimensional superlattice structure using the atomic coordinates determined by neutron and X-ray diffraction (Gao et al., 1993). We assumed that the holes were evenly distributed in CuO_2 plane, while electrons in the BiO plane were modulated along the *b*- and *c*-axis with a body-centered symmetry, as shown in Fig. 5(a), where the large dots for electrons e^- represent high occupancy. With reference to formal valence, this model shows a pileup of

Table 1
Charge assignments for $YBa_2Cu_3O_7$ and $Bi_2Sr_2CaCu_2O_8$, based on formal valence and models from electronic-structure calculations

$YBa_2Cu_3O_7$							
Model	Y	BaO		CuO_2		CuO	
		Ba	O	Cu	O	Cu	O
Pickett	+ 3	+ 2	− 1.69	+ 1.62	− 1.69	+ 1.62	− 1.69
Ionic	+ 3	+ 2	− 2	+ 2	− 2	+ 2	− 1
$Bi_2Sr_2CaCu_2O_8$							
Model	Ca	BiO		SrO		CuO_2	
		Bi	O	Sr	O	Cu	O
Gupta	+ 1.598	+ 0.996	− 0.887	+ 1.786	− 1.36	+ 1.647	− 1.4905
Ionic	+ 2	+ 3	− 2	+ 2	− 2	+ 2	− 2

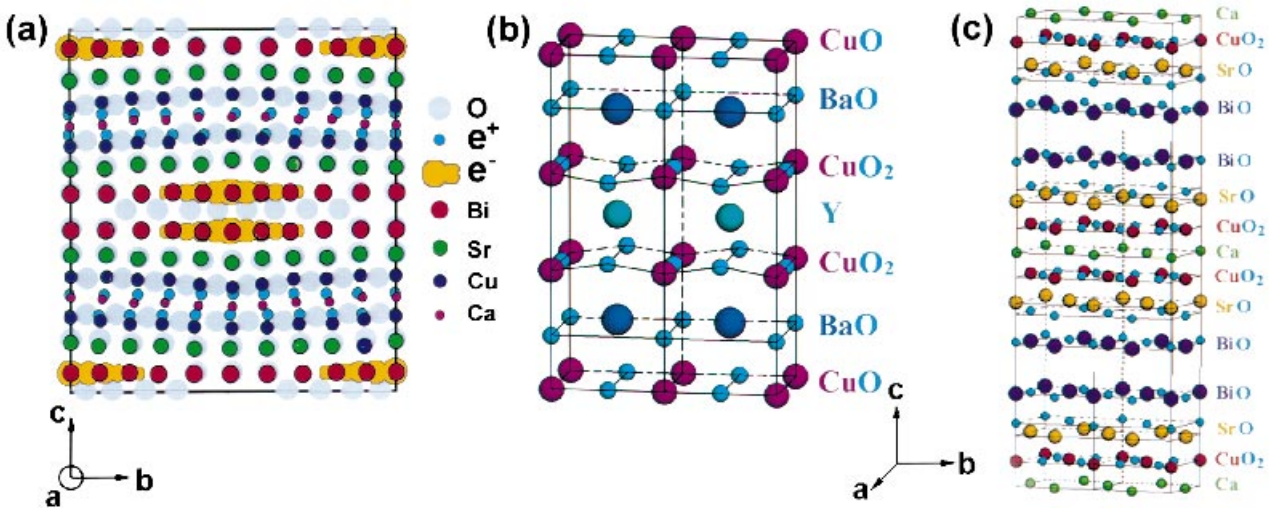

Fig. 5. (a) Structure model of the supercell ($0.54 \times 2.6 \times 3.1$ nm^3) projected along the *a*-axis in Bi/2212. Both lattice displacement and charge ordering associated with the modulation are included. For electron, e^-, the large circles correspond to high occupancy; (b) crystal structure of $YBa_2Cu_3O_7$; (c) and Bi/2212, showing their layer characteristics along the *c*-axis.

electron charge in the region of the BiO double layer where the atomic planes expand along the c-direction; this agrees with the notion that electron doping increases the Bi–O distance (Pham et al., 1993). The embedded image in Fig. 4 is a calculated image, based on the structural model shown in Fig. 5(a), and matches well with the experimental observation. A crystal thickness of 2.7 nm and objective-lens defocus of -50 nm were used in the calculation. Comparison with the calculated images based on models consisting of neutral atoms suggests that the black-cage contrast is indeed associated with electron charge-cluster in the BiO layers. Such a charge modulation was related to charge stripes in Bi/2212 to understand superconductivity mechanism (Bianconi et al., 1996).

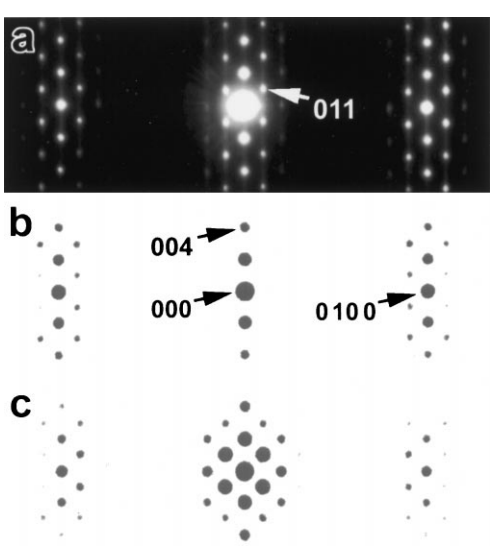

Fig. 6. Selected area diffraction pattern in a thin Bi/2212 crystal: (a) experimental observation; (b) calculated pattern based on the model consisting of neutron atoms; and (c) calculated pattern based on the model consisting of charge atoms, as shown in Fig. 5(a).

Interpretation of high-resolution images is often complicated since they strongly depend on imaging conditions, and some of the experimental parameters, such as thickness and defocus, are difficult to determine. In contrast, interpretation of diffraction is rather straightforward. Fig. 6(a) shows a selected area diffraction pattern of the (100) zone of Bi/2212. The superlattice reflections are clearly visible. We emphasize that even in very thin areas where multiple scattering is negligible, the intensity of the super-reflections near the forward direction, such as 011, are quite strong. These super-reflections should not be visible in a kinematical diffraction pattern if the superlattice is formed solely by the displacive modulation, and the associated displacements are not extremely large.

Fig. 6(b) and (c) are calculated diffraction patterns for neutral atoms and charged atoms, respectively for neutral atoms and charged atoms, based on many-beam dynamical diffraction theory. The difference is significant. The diffraction pattern for neutral atoms only shows the sublattice (00*l*) reflections near the forward direction, and the 011 reflections of the superlattice are invisible. This is in good agreement with Fig. 3, since displacive modulation should not alter the intensity of the reflections at small scattering angles. Nevertheless, the diffraction pattern calculated for charged atoms shows strong intensity for the 011 and 022 superlattice reflections (Fig. 6(c)), consistent with the experimental observation shown in Fig. 6(a). Thus, it is clear that, for a very thin crystal, the innermost superreflections visible near the forward direction result from the charge component of the modulation.

The intrinsic difference in intensity distribution of the inner reflections in the selected area diffraction patterns in Fig. 6(b) and (c) also suggests a significant change in the

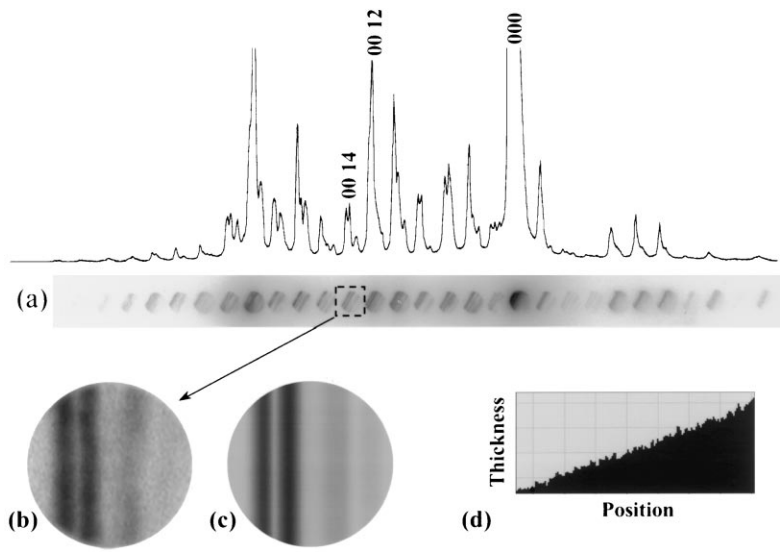

Fig. 7. (a) Experimental PARODI pattern of the (00*l*) systematic row, showing diffraction intensity as a function of crystal thickness in Bi/2212. A line scan of the intensity is also included. (b) An enlarged disk of the 0014 reflection. Note, the disk is rotated anti-clockwise about 20° from (a), and the thickness increases from left to right. (c) Calculated intensity of the disk pattern (b) based on many-beam dynamic diffraction theory. (d) A line scan from a thick map, mapped using electron energy-loss spectroscopy, showing the linear increase in the thickness of a wedge we studied.

superlattice image, if a very small aperture covering only the innermost super-reflections is used to image the modulation. Inverse Fourier transformation of Fig. 6(b) gave only a one-dimensional lattice image along the *c*-axis, while for Fig. 6(c), a two-dimensional lattice pattern was generated. As reported previously (Zhu and Tafto, 1996), careful experiments using such a small aperture in very thin crystal regions did show two-dimensional body-centered superlattice images when the crystal was viewed along the *a*-axis, in agreement with the black-cage pattern in Fig. 4.

5. Quantitative measurements of charge density and charge transfer

Because high-resolution images change with imaging conditions, quantitative measurements of charge distribution still rely on diffraction experiments (Gjonne and Boe, 1993). Efforts to study charge distribution using electron diffraction can be traced back to early 70s (Anstis et al., 1973). In recent years, convergent electron beam diffraction (CBED) techniques, especially with the aid of a field-emission source and energy filter, have been used to accurately determine structure factors by comparing detailed features (e.g. the intensity and position of high-order-Laue-zone lines) in the observed and calculated CBED disks (Tsuda and Tanaka, 1995; Terasaki et al., 1979; Vincent et al., 1984). Such quantitative, high precision CBED studies can reveal important information about bonding and ionicity for small unit-cell crystals (Zuo et al., 1988; Zuo, 1993; Matsuhata et al., 1994; Zuo et al., 1997).

Conventional CBED techniques are not suitable for studying crystals with a large-unit-cell, partly because of the overlap of the CBED disks. In determining charge distribution for high-temperature superconductors, we recently developed a new CBED method to simultaneously record diffraction intensity of many reflections as a function of crystal thickness (Zhu and Tafto, 1997; Tafto et al., 1998). Unlike conventional CBED methods, which focus the probe on the sample to retrieve structural information for different beam orientations, we focus the electron probe above or below the sample. By doing so, we were able to form shadow image for many reflections simultaneously, that contain not only orientation information, but also thickness profile, or *Pendellösung* plots. The thickness profile usually starts from zero up to a maximum that can range from 10 nm to several hundred nanometers, depending on the distance from the specimen to the beam crossover. Fig. 7(a) is an experimental shadow-image or a diffraction pattern from a wedge Bi/2212 crystal, using the Fuji Imaging Plate system with our new 300 kV JEOL 3000F field-emission microscope, together with a line scan of the intensity shown above. Because of the short reciprocal vectors along the c^*-axis, we achieve parallel recordings of oscillating diffraction intensities (PARODI) as a function of thickness and excitation error (or incident-beam direction) for 30 reflections in a one-second exposure. The orientation of the edge of the wedge relative to the reciprocal-lattice row is unimportant, but it is most convenient to make a line scan when the edge is normal to the **g**. In each disk in Fig. 7(a), the top-left side of the shadow image corresponds to vacuum, as easily seen in the 000 disk. Fig. 7(b) shows an enlarged diffraction disk of the 0014 reflection from Fig. 7(a), after a $\sim 20°$ anti-clockwise rotation, and is compared with a calculated one (Fig. 7(c)). The thickness in the disk increases from left to right. The intensity oscillation, or

Pendellösung fringes, originates from the increase of thickness, and its period normal to the wedge scales with the extinction length.

There are distinct advantages of our PARODI method: (1) dozens of reflections (30 reflections in Fig. 7(a)) in large unit-cell crystals can be recorded simultaneously, thereby ensuring that the exposure and the crystallographic direction of the incident beam are exactly the same for all reflections; (2) the increase in intensity can be followed at a very small thickness, where the relationship between the structure factors and the intensities is simple, and where the problems of normal and anomalous absorption are minimized; (3) since the probe is not focused on the sample, the beam damage is much less than in conventional CBED; (4) the discrete data-points in each reflection acquired from different thicknesses are considered to be independent, due to the strong dynamical coupling of the different diffracted beams, resulting in a very high ratio of the number of observations vs the number of variables. This is very important in the fitting process giving a high level of confidence.The intensity distribution of the shadow image within the disks depends strongly on the crystal thickness. To simplify the analysis, an ideal wedge with a linear increase in thickness is desirable. If we start from zero thickness, the linear increase in thickness warrants the possibility of using only one additional variable, the maximum thickness t_{max}, to obtain a large number of intensity data points for different thicknesses. In practice, a good wedge is not very difficult to find, especially when the probe is close to the sample, or the illuminated area is small. The shape of a wedge can be revealed by acquiring a thickness map of the area of interest using an electron energy-loss spectroscopy, based on the relationship $t = \lambda \ln(I_t/I_0)$, where t is the thickness, I_0 the integrated intensity of zero-loss peak, I_t the total intensity of the spectrum, and λ the inelastic mean free-path of the crystal. Fig. 7(d) is a line scan from a thickness map, t/λ, showing the linear increase in thickness of a wedge we studied.

The intensity distribution of the shadow image also depends on excitation error, as in the conventional CBED. For the (00*l*) reflections in high-temperature superconductors, the influence of the excitation error to the intensity distribution is very small, however, because of the small convergent beam angle we had to use to avoid overlap of the reflection disks. It is evident from Fig. 7(b) and (c) that there is little variation in intensity with respect to the change in the excitation error, or to the change of the position within the disks along the direction parallel to the specimen edge, where the thickness of the crystal is constant. Thus, with the crossover of the beam away from the specimen, a line-scan perpendicular to the edge of the wedge gives intensity oscillations mainly as a function of the crystal thickness.

Our goal is to determine the valence-electron distribution in the crystals from electron diffraction data, especially the structure factors of the low-order reflections that are very sensitive to the rearrangement of the charge. We measured structure factors from electron diffraction experiments, then converted $F^e_{\mathbf{g}}$ to $F^x_{\mathbf{g}}$ before performing the inverse Fourier transform using Eq. (1) to obtain the charge density ρ. In SI unit, the conversion can be expressed as:

$$F^x_{\mathbf{g}} = \sum_i Z_i \exp(-B_i s^2) \exp(-2\pi i \mathbf{g}\cdot\mathbf{r}) - 41.78 s^2 F^e_{\mathbf{g}}. \quad (8)$$

The inaccuracy of X-ray structure factors at small scattering angle in determining valence-electron distribution is attributed to the large number of total electrons in the unit-cell. What is important for us is the difference between the measured structure factors and those calculated for ions of formal valency. We thus avoid the large contribution from the core electrons when we convert back from the difference in structure factors between the measurement and ionic model for electrons to that for X-rays to obtain $\Delta\rho$ in Eq. (3):

$$F^x_{\mathbf{g}m} - F^x_{\mathbf{g}f} = -41.78 s^2 (F^e_{\mathbf{g}m} - F^e_{\mathbf{g}f}). \quad (9)$$

To quantify the intensity oscillation, we calculated the shadow image of the reflections using many-beam dynamical multislice, as well as the Bloch wave approach. We found that although both approaches gave similar results, the multislice approach is easier for image calculations, while the Bloch-wave approach is easier for diffraction calculations. For this approach, the intensity of the diffracted beam in a thin crystal can be expressed as (Howie, 1978):

$$I_{\mathbf{g}} = \sum_{j,j'} C_0^{(j)} C_{\mathbf{g}}^{(j)} C_0^{(j')*} C_{\mathbf{g}}^{(j')*} \exp[2\pi i(\gamma^{(j)} - \gamma^{(j')})z] \exp(-\mu z) \quad (10)$$

where μ is an absorption parameter and z the crystal thickness. $C_{\mathbf{g}}^{(j)}$ represents the gth excitation coefficient of the jth Bloch wave and * denotes complex conjugate. γ and $C_{\mathbf{g}}^{(j)}$ are eignvalues and eigenvectors to be determined by the relation $AC_g = \gamma C_g$; here, A is the structure matrix whose off-diagonal elements depend on the crystal potential and diagonal elements on the orientation of the incident beam. We developed our own computer codes, and the calculations usually included more than 50 reflections.

We compare the measured intensity-thickness profiles with calculated ones. We then refined the measurements by systematically changing the charge distribution in calculations, and thus, the structure factor of the low-order reflections, until good agreement was achieved. To evaluate the goodness of the agreement, we also developed an error analysis procedure to derive the "best fit" between calculated and observed intensities. We use the R factor defined by:

$$R = \frac{\sum_{\mathbf{g}_i, t_j} |I_{obs} - I_{cal}|}{\sum_{\mathbf{g}_i, t_j} |I_{obs}|} \times 100\%$$

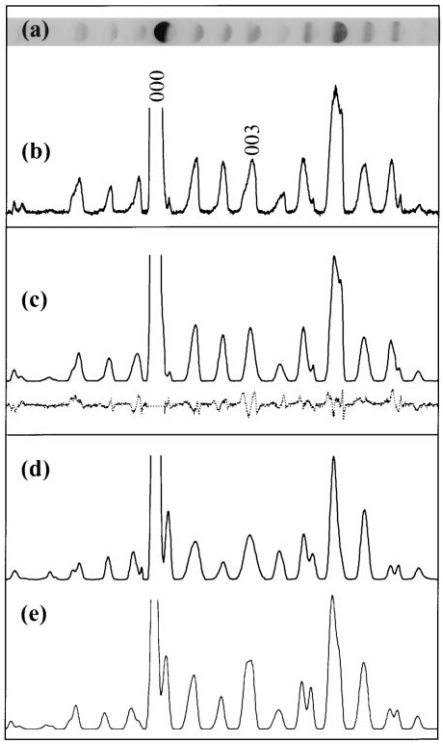

Fig. 8. (a) Experimental PARODI pattern of the (001) system row in $YBa_2Cu_3O_7$; (b) a line scan of the intensity from (a); (c) calculated intensity profile with the best fit to the experiment, together with the difference profile; (d) calculated intensity profile based on the Gupta model; and (e) calculated intensity profile based on the Pickett model.

where g_i ($i = 1, 2, \ldots$) is the reciprocal lattice and t_j ($j = 1, 2, \ldots, 50$) represents the partition of the specimen thickness. We note that this R factor differs from the one used in traditional crystallography (Rietveld, 1969), where no variation with thickness is considered. In our approach, the discrepancies between calculated and observed intensities were summed up over all reflections and thicknesses. Because the diffraction intensity is very sensitive to the thickness, fitting the intensity profile for the entire range of thickness is not a trivial task. The resulting R may not be a small value. However, the "best fit" is chosen when a global minimum value of R is reached.

6. The valence-electron distribution of $YBa_2Cu_3O_7$ and $Bi_2Sr_2CaCu_2O_{8+\delta}$

Fig. 5(b) and (c) shows the crystal structure of $YBa_2Cu_3O_7$ and $Bi_2Sr_2CaCu_2O_{8+\delta}$, respectively, both consisting of sequence of layers along the c-axis. Since we limited our study to the intensity profiles of the (00l) systematic reflection row, only the charge transfer between the layers was investigated. Table 1 shows the charge assignments based on first-principle electronic-structure calculations by Pickett (1989) and Gupta and Gupta (1991; 1994). Note, for $YBa_2Cu_3O_7$, the assigned charge by the Gupta model for Cu and O varies with their constituent atom in the plane, while, by the Pickett model, identical charge was assigned to the same element. For

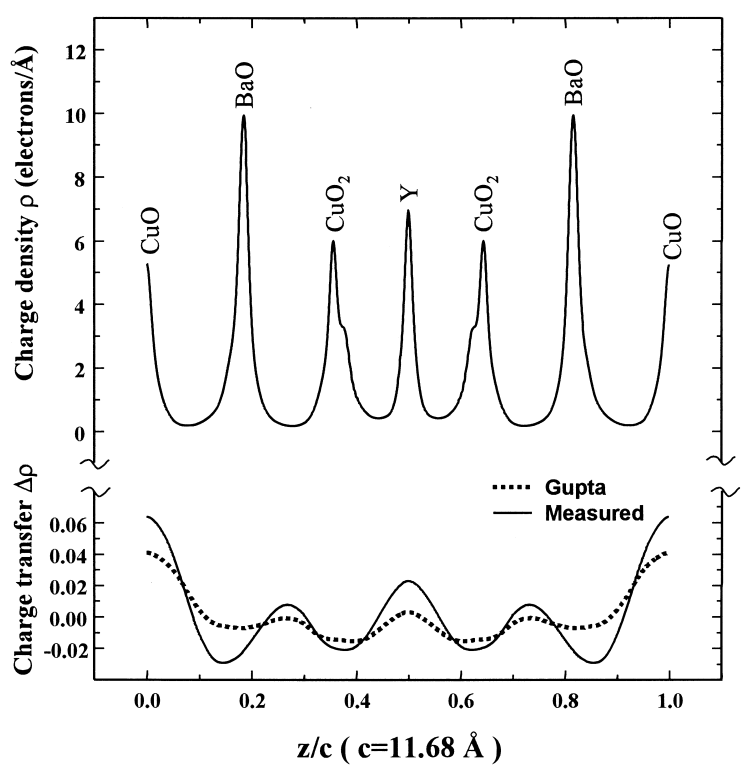

Fig. 9. Plot of charge-density distribution ρ along the c-axis for $YBa_2Cu_3O_7$, together with the plot of charge transfer $\Delta\rho$ derived from the measurement, and the Gupta mode using formal valence as a reference.

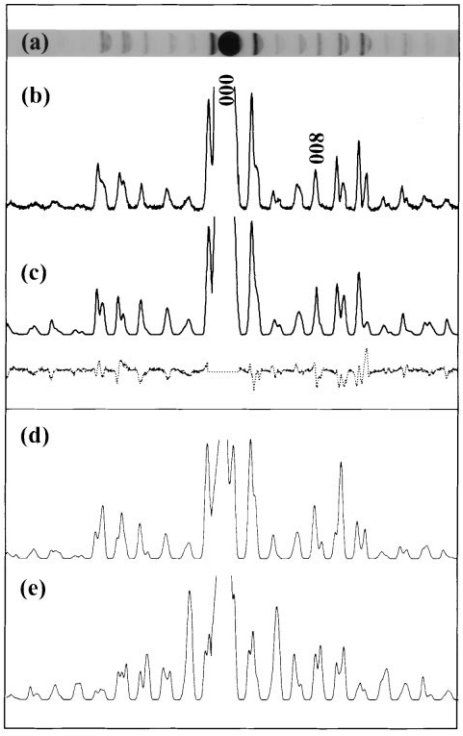

Fig. 10. (a) Experimental PARODI pattern of the (001) system row in Bi/2212; (b) a line scan of the intensity from (a); (c) calculated intensity profile with the best fit to the experiment, together with the difference profile; (d) calculated intensity profile based on the Gupta model; and (e) calculated intensity profile based on the ionic model.

comparison, the formal valence assigned for the ionic model of Bi^{3+}, Sr^{2+}, Ca^{2+}, Y^{3+}, Ba^{2+}, Cu^{2+}, O^{-} and O^{2-} was also included in the table. In the calculations, we used atomic positions that were determined by neutron and X-ray diffraction (Jorgensen et al., 1990; Gao et al., 1993), and the scattering amplitudes for X-ray diffraction from the International Tables of Crystallography (1992) for most atoms and ions, but for O^{2-} we used values of Rez et al. (1994). We converted these amplitudes to scattering amplitudes for electrons by the Mott formula.

6.1. $YBa_2Cu_3O_7$

Fig. 8(a) shows an experimental PARODI pattern of the 00*l* reciprocal lattice row in a nominal $YBa_2Cu_3O_7$ sample. The corresponding line scan is shown in Fig. 8(b), after subtracting background around the strong beam in the forward direction. The thickness range was 0–50 nm, with (003) as the center of the Laue circle. Fig. 8(c) is the calculated intensity profiles with the best fit to the experiment. Adjustable experimental parameters were the thickness range, the incident beam direction, and absorption parameters.

We compared the experiments with two charge distribution models based on first-principle calculations by Pickett (1989) and Gupta and Gupta (1991), as shown in Fig. 8(d) and (e), respectively. The calculated intensity profiles for both models show poor agreement with the experiment (Fig. 8(b)). For instance, the intensity variation at the thickness range of 40–60 nm in the 000 disk, which is very sensitive to the charge distribution, does not agree with the experiment. The agreement for the ionic model is even worse. Through an error analysis procedure, the *R* value we calculated for the ionic model was 50.7, and 40.2 and 43.8 for the Gupta and Pickett model, respectively. We note that the calculated intensity could be brought within an acceptable range of the experimentally measured one by extremely small adjustments to the models' structure factors of the low-order reflections, which illustrate great sensitivity of the electron diffraction to the charge distribution. The values of the electron structure factors of the 001 and 002 of $YBa_2Cu_3O_{7-\delta}$ change drastically, in going from a purely ionic model to the model based on the electronic structure calculation. On the other hand, structure factors of reflections farther out in reciprocal space are only modestly influenced by the valence-electron distribution. However, the sensitivity of electron diffraction at these low angles is so high that by making the small changes relative to the model (Gupta and Gupta, 1991) indicated in Fig. 8(d), the calculated diffraction patterns approached the experimental ones with the smallest *R* value of 16.8. Relative to the Pickett model (Pickett, 1989), this modification amounts to moving per unit-cell, 0.3 electrons from the BaO layer to the Y layer, and 0.05 electrons from the CuO_2 layer to the CuO layer. Based on the best fit, we obtained the 001 and 002 structure factors to the values -3.4 ± 0.9 and -4.0 ± 1.1 Å, respectively. These accuracies in electron diffraction correspond to accuracies of the X-ray structure factors of 0.1 and 0.4 electron, respectively.

Fig. 9 plots the measured charge density ρ for $YBa_2Cu_3O_7$, with the horizontal axis as the position of the (00*l*) lattice planes for one unit-cell. Note, the shoulder on intensity peak in the CuO_2 plane results from the small deviation of the Cu and O sites projected on to the *c*-axis. The charge-density plot suggests that BaO planes have large number of total electrons, while the electron densities in the CuO, CuO_2 and Y plane are similar, about 60% of that in the BaO plane. Fig. 9 also shows the difference charge-density profiles between the Gupta model and the ionic model, and that between the measurements and the ionic model. They represent the charge transfer $\Delta\rho$, or valence-electron distribution, in the crystal using formal valence as a reference. Integrating both difference profiles over the unit-cell of 1.168 nm along the *c*-axis results in a zero net-charge-transfer, suggesting charge neutrality over the dimension of the unit-cell. The difference profiles indicate that there is an appreciable discrepancy between the Gupta model and the measured valence-electron distribution. The charge transfer in the Y and BaO planes in the Gupta model is quite small, as expected from the model in which these planes are nearly fully ionic in character, while our measurements show that there is significant excess of electrons in the Y and deficiency of electrons in the BaO plane. The relatively large

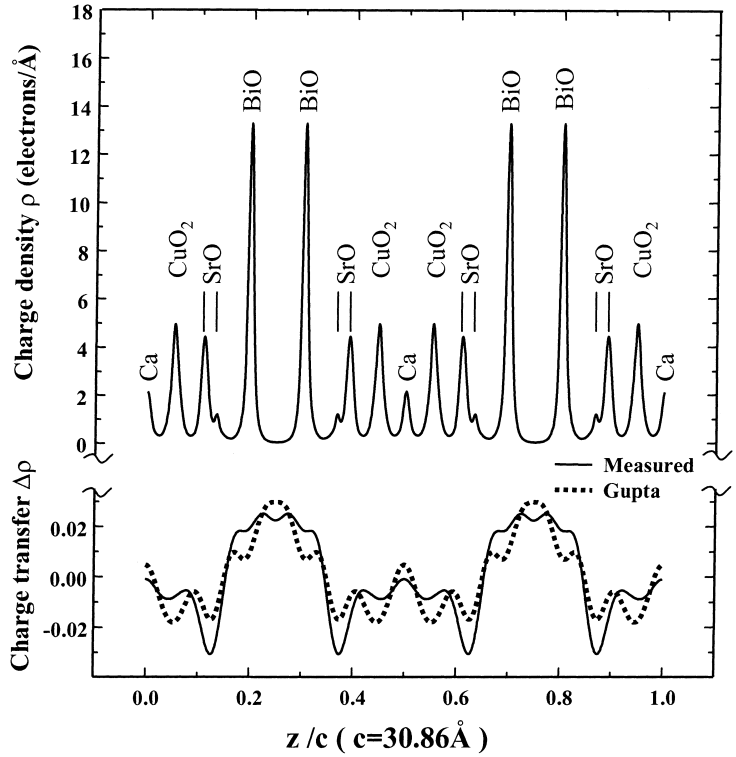

Fig. 11. Charge density distribution ρ along the c-axis for Bi/2212 together with the charge transfer $\Delta\rho$ determined from the measurement and the Gupta model, using formal valence as a reference.

positive value of $\Delta\rho$, especially the measured one, in the CuO chain planes implies that sufficient electrons are transferred into the planes. This transfer apparently is mainly from the CuO_2 planes, but may also be from the BaO planes. For $YBa_2Cu_3O_7$, Brown (1991) concludes, using bond-valence considerations on the crystallographic data from neutron diffraction (Jorgensen et al., 1990) that we used in this study, that there are 0.3 electron holes per CuO_2 unit in the CuO_2 planes. The electronic structure calculations Pickett (1989) and Gupta and Gupta (1991) suggest 0.24 and 0.28 holes, respectively, and our experimental study suggests 0.25 electron holes per CuO_2 unit.

6.2. $Bi_2Sr_2CaCu_2O_{8+\delta}$

Fig. 10(a) is an experimental PARODI pattern, showing the variation of the diffraction intensities with the thickness for the (00l) reflections in $Bi_2Sr_2CaCu_2O_{8+\delta}$. The illuminated area covers a thickness range of 0–60 nm (t_{max} = 60 nm) with the center of the Laue circle at 001. The corresponding line scan of the intensity in Fig. 10(a) is shown in (b). Fig. 10(c) shows the calculated intensity using 51 beams with the best fit of the 002 and 004 structure factors with R = 16.9. The agreement for areas with small t_{max} usually is better, because there is a much less dynamical coupling of the diffracting beams, as we reported previously for t = 0–6 nm (Wu et al., 1999). Note, a small deviation in the intensity of high-order reflections, such as 0012, in certain thickness range between the experiment, and the best fit has insignificant influence on the accuracy of the measurement of the charge distribution. The calculated intensity (Fig. 10(d)) based on the Gupta model (Gupta and Gupta, 1994) shows small deviation with the experiment, with R = 39.3. In contrast, the purely ionic model can be completely ruled out because its intensity of the 002 reflection is too low, while that of the 004 is much too high, the R value we derived reaches 79.6. The best-fit intensity profile to the experiment, Fig. 10(c), was achieved by a very small adjustment to the intensity profile of the Gupta model, Fig. 10(d), moving 0.144 electron from the SrO layer to the BiO layer and 0.056 electron from the SrO layer to the CuO_2 layer per unit-cell. Through quantitative refinement, we concluded that for $Bi_2Sr_2CaCu_2O_8$ the value of the structure factor of the 002 and 004 reflection are $+15 \pm 10$ and -5 ± 5 Å, which after conversion to X-ray structure factors, are -157.9 ± 0.4 and 1.65 ± 0.8 electrons, respectively.

Fig. 11 shows the measured charge distribution ρ along the c-axis in Bi/2212 over one unit-cell dimension. The lattice planes are labeled above the charge density peaks. We note that there is a high, well-separated electron-density distribution around the double BiO layers and very low density in CaO. The density in the CuO_2 and SrO layers are similar, less than half of that in the BiO layers. Below the charge-density plot are two difference charge-density profiles, showing the discrepancy in charge transfer $\Delta\rho$ based on the measurements and the Gupta model, using

the formal valence as a reference. Both the Gupta model and the experimental observations indicate excess valence electrons associated with the BiO double layer, consistent with the HREM observations. It is interesting that the highest charge transfer occurs in the interstitial position, rather than in the BiO layers, suggesting possible covalent-bonding character of the BiO double layers. Both profiles also indicate that Ca is nearly completely ionic with negligible charge transfer, similar to the Y plane in $YBa_2Cu_3O_7$. There are some minor differences between the Gupta model and the experimental observations. The $\Delta\rho$ profile from the measurement implies that the valence distribution in the CuO_2 and SrO planes is near equal, while that from the Gupta model suggests that there are more electron transferred into the SrO plane than into the CuO_2 plane.

7. Conclusion

We demonstrated that high-energy electron probe is one of the most sensitive techniques for determining structure factors and charge distribution at small scattering angles. It can be used to study extremely small changes in the valence-electron distribution, even in complex crystals containing atoms of high atomic numbers with a high density of core electrons, such as the high-temperature superconductors. For example, the movement of 0.05 electron holes per unit-cell of $YBa_2Cu_3O_7$ between the CuO chain and the CuO_2 plane that corresponds to rearranging 1 out of 5000 electrons in the crystal, changes the 001 structure factor of electron diffraction by 1 Å, while we determine this structure factor with an accuracy of 0.9 Å. Electron diffraction and imaging, especially combined with electron energy-loss spectroscopy, can be a unique and powerful tool to reveal electronic structure of materials of complex systems.

Acknowledgements

The research was supported by the US Department of Energy, Division of Materials, Office of Basic Energy Science, under Contract No. DE-AC02-98CH10886.

References

Brown, I.D., 1991. The influcnce of internal strain on the charge distribution and superconducting transition temperature in $Ba_2YCu_3O_4$. J. Solid State Chem. 90, 155.

Bianconi, A., Lusignoli, M., Saini, N.L., Bordet, P., Kvick, A., Radailli, P.G., 1996. Stripe structure of the CuO_2 plane in $Bi_2Sr_2CaCu_2O_{8+y}$ by anomalous X-ray diffraction. Phys. Rev. B 54, 4310–4314.

Fink, J., Nucker, N., Pellegrin, E., Romberg, H., Alexander, M., Knupfer, M., 1994. Electron energy-loss and X-ray absorption spectroscopy of curate superconductors and related compounds. J. Electron Spectrosc. Related Phenom. 66, 395–452.

Gajdardziska-Josifovska, M., McCartney, M., DeRuijter, W.J., Smith, D.J., Weiss, J.K., Zuo, J.M., 1993. Accurate measurements of meaning inner potential of crystal wedges using digital electron holography. Ultramicroscopy 50, 285–299.

Gao, Y., Coppens, P., Cox, D.E., Moodenbaugh, A.R., 1993. Combined X-ray single-crystal and neutron powder refinement of modulated structures and application to the incommensurately modulated structure of $Bi_2Sr_2CaCu_2O_{8+y}$. Acta Cryst. A49, 141–148.

Gemming, T., Mobus, G., Exner, M., Ernst, F., Ruhle, M., 1997. Ab initio HRTEM simulations of ionic crystals: a case study of sapphire. J. Microscopy 190, 89–98.

Gjonne, K., Boe, N., Tafto, J., 1993. Distribution of holes in $YBa_2Cu_3O_7$ form convengent beam electron diffraction. Ultramicroscopy 48, 37–41.

Gupta, R.P., Gupta, M., 1991. Order-disorder-driven change in hole concentration and superconductivity in $YBa_2Cu_3O_{6.5}$. Phys. Rev. B 44, 2739–2746.

Gupta, R.P., Gupta, M., 1994. Electronic-structure calculation of the hole-carrier-density distribution in $Bi_2Sr_2CuO_6$, $Bi_2Sr_2CaCu_2O_8$, and $Bi_2Sr_2Ca_2Cu_3O_{10}$ superconductors. Phys. Rev. B 49, 13154–13159.

Horiuchi, S., Maeda, H., Tanaka, Y., Matsui, Y., 1988. Structure analysis of the $Bi_2(Sr, Ca)_3Cu_2O_{8.2}$ superconducting crystal based on the computer simulation of HRTEM images. Jpn. J. Appl. Phys. 27, L1172–L1174.

Howie, A., 1978. High voltage electron microscopy: the theory of high energy electron diffraction. In: Amelinckx, S., Gevers, R., Van Landuyt, J. (Eds.). Diffraction and Imaging Techniques in Materials Science, North-Holland, Amsterdam, pp. 457.

1992. International Tables of Crystallography, C, Kluwer Academic, Dordrecht pp. 475–499.

Imai, K., Nakai, I., Kawashima, T., Sueno, S., Ono, A., 1988. Single crystal X-ray structure analysis of $Bi_2(Sr, Ca)_2CuO_x$ and $Bi_2(Sr, Ca)_3Cu_2O_x$ superconductors. Jpn. J. Appl. Phys. 27, L1661–L1664.

Jorgensen, J.D., Veal, B.W., Paulikas, A.P., Nowicki, L.J., Crabtree, G.W., Claus, H., Kwok, W.K., 1990. Structure properties of oxygen-deficient $YBa_2Cu_3O_{7-\delta}$. Phys. Rev. B 41, 1863–1877.

Matsuhata, H., Gjonnes, J., Tafto, J., 1994. A study of structure factors in rutile-type SnO_2 by high-energy electron diffraction. Acta Cryst. A50, 115–122.

Matthias, B.T., 1957. Superconductivity in the periodic system. Prog. Low Temp. Phys. 2, 138–150.

Nucker, N., Pellegrin, E., Schweiss, P., Fink, J., Molodtsov, S.L., Simmons, C.T., Kaindl, G., Frentrup, W., Erb, A., Muller-Vogt, G., 1995. Site-specific and doping-dependent electronic structure of $YBa_2Cu_3O_x$ probed by O 1s and Cu 2p X-ray-absorption spectroscopy. Phys. Rev. B 51, 8529–8540.

Nücker, N., Romberg, H., Xi, X.X., Fink, J., Gegenheimer, B., Zhao, Z.X., 1989. Symmetry of holes in high-T_c superconductors. Phys. Rev B 39, 6619–6629.

Pham, A.Q., Studer, F., Merrien, N., Maignan, A., Michel, C., Raveau, B., 1993. Complex influence of the Bi–O reservior and oxygen nonstoichiometry on the hole density in $Bi_2Sr_2CaCu_2O_8$. Phys. Rev. B 48, 1249–1253.

Pickett, W.E., 1989. Electronic structure of the high-temperature oxide superconductors. Rev. Mod. Phys. 6, 433–512.

Rez, D., Rez, P., Grant, I., 1994. Dirac–Fock calculations of X-ray scattering factors and contributions to the mean inner potential for electron scattering. Acta Cryst. A50, 481–497.

Rietveld, H.M., 1969. A profile refinement method for nuclear and magnetic structures. J. Appl. Cryst. 2, 65–71.

Tafto, J., Zhu, Y., Wu, L., 1998. A new approach towards measuring structure factors and valence-electron distribution in crystals with large unit-cells. Acta Cryst A54, 532–542.

Terasaki, O., Watanabe, D., Gjonnes, J., 1979. Determination of crystal structure factors of Si by the intersecting-Kikuchi-line method. Acta Cryst. A35, 895–900.

Tsuda, K., Tanaka, M., 1995. Refinement of crystal structure parameters using convergent-beam electron diffraction: the low temperature phase of $SrTiO_3$. Acta Cryst. A51, 7–19.

Tranquada, J.M., Sternlieb, B.J., Axe, J.D., Nakamura, Y., Uchida, S.,

1995. Evidence for stripe correlation's of spins and holes in copper oxide superconductors. Nature 375, 561.

Vincent, R., Bird, D.M., Steeds, J.W., 1984. Structure of AuGeAs determined by convergent-beam electon diffraction II: refinement of structural parameters. Philos. Mag. A50, 765–786.

Wu, L., Zhu, Y., Tafto, J., 1999. Test of first-principle calculations of charge transfer and electron-hole distribution in oxide superconductors by precise measurements of structure factors. Phys. Rev. B 59, 6035–6038.

Zhu, Y., Tafto, J., 1996. Direct imaging of charge modulation. Phys. Rev. Lett. 76, 443–446.

Zhu, Y., Tafto, J., 1997. Measurement of charge transfer in $YBa_2Cu_3O_7$ using novel electron diffraction method. Philos. Mag. B75, 785–791.

Zuo, J.M., O'Keefe, M., Rez, P., Spence, J.C.H., 1997. Charge density of MgO: implications of precise new measurements for theory. Phys. Rev. Lett. 78, 4777–4780.

Zuo, J.M., Spence, J.C.H., O'Keeffe, M., 1988. Bonding in GaAs. Phys. Rev. Lett. 61, 353–356.

Zuo, J.M., 1993. Automated structure-factor refinement from convergent-beam electron diffraction patterns. Acta Cryst. A49, 429–435.